

Persistent cloud cover over mega-cities linked to surface heat release

Article

Published Version

Creative Commons: Attribution 4.0 (CC-BY)

Open Access

Theeuwes, N. E. ORCID: <https://orcid.org/0000-0002-9277-8551>, Barlow, J. F., Teuling, A. J., Grimmond, C. S. B. ORCID: <https://orcid.org/0000-0002-3166-9415> and Kotthaus, S. (2019) Persistent cloud cover over mega-cities linked to surface heat release. *npj Climate and Atmospheric Science*, 2. 15. ISSN 2397-3722 doi: <https://doi.org/10.1038/s41612-019-0072-x> Available at <https://centaur.reading.ac.uk/83524/>

It is advisable to refer to the publisher's version if you intend to cite from the work. See [Guidance on citing](#).

To link to this article DOI: <http://dx.doi.org/10.1038/s41612-019-0072-x>

Publisher: Nature Publishing Group

All outputs in CentAUR are protected by Intellectual Property Rights law, including copyright law. Copyright and IPR is retained by the creators or other copyright holders. Terms and conditions for use of this material are defined in the [End User Agreement](#).

www.reading.ac.uk/centaur

CentAUR

Central Archive at the University of Reading

Reading's research outputs online

ARTICLE OPEN

Persistent cloud cover over mega-cities linked to surface heat release

Natalie E. Theeuwes¹, Janet F. Barlow¹, Adriaan J. Teuling², C. Sue B. Grimmond¹ and Simone Kotthaus^{1,3}

Urban areas are a hotspot for the interactions between the built environment, its inhabitants, and weather. Unlike the impact of temperatures through the well-known urban heat island effect, urban effects on cloud formation remain unknown. In this study we show observational evidence of a systematic enhancement of cloud cover in the afternoon and evening over two large metropolitan areas in Europe (Paris and London). Long-term measurements in and around London show that during late-spring and summer, even though less moisture is available at the surface and the atmosphere is drier, low clouds can persist longer over the urban area as vertical mixing of the available moisture is maintained for a longer period of time, into the evening transition. Our findings show that urban impacts on weather extend beyond temperature effects. These prolonged clouds over the city might enhance the urban heat island via night-time radiative forcing.

npj Climate and Atmospheric Science (2019)2:15; <https://doi.org/10.1038/s41612-019-0072-x>

INTRODUCTION

A growing fraction of the global population lives in cities.¹ These cities can profoundly influence their atmospheric environment. The most commonly studied impact is the urban heat island effect (UHI), i.e., cities generally have a higher air temperature at street level during the evening and into the night than their surroundings.^{2–4} After extensive research, the key drivers and dynamics of the UHI are understood reasonably well. However, it is uncertain how the urban surface influences the atmospheric processes leading to clouds and convection. Previous studies have found cities influence individual mesoscale convective systems, based on case studies of convective precipitation^{5,6} or idealised high-resolution simulations.^{7,8} Although clouds are associated with convection and precipitation, only a few studies examine cloud cover over cities.^{9–11} In addition, clouds alter radiative forcing and thereby the thermal climate.

Surface energy balance partitioning between moisture (latent heat) and sensible heat fluxes influences the formation and maintenance of boundary-layer clouds.^{12,13} Surface energy balance partitioning over cities differs from the rural surroundings,² with latent heat fluxes generally lower above urban areas as vegetation is replaced by built surfaces. Hence, energy is predominantly partitioned into the heating of the building volume (storage heat flux) and the atmosphere (sensible heat flux).^{14,15} Cities are further expected to influence boundary-layer clouds through their rougher surface (e.g. buildings and trees) causing frictional convergence and the release of aerosols resulting in more cloud condensation nuclei.¹⁶

This study explores whether, and to what extent, cloud dynamics are different over cities compared to their surroundings. Observations from the high-resolution visible broadband channel of Meteosat Second Generation (MSG-HRV)¹⁷ are used at a resolution of ~1–2 km, for two large metropolitan areas in Europe: Paris (~11.8 million inhabitants in the functional urban area¹⁸) and

London (~12.3 million inhabitants in the functional urban area¹⁸). The cloud identification method neither distinguishes precipitating from non-precipitating, nor high from low clouds. However, from long-term ground-based measurements in London^{19,20} we can distinguish low, non-precipitating clouds, examine night-time clouds and identify some of the hypothesised causes of urban-rural cloud occurrence differences. Combining ground-based and space-borne observations provides a detailed picture of the interaction between the urban surface and cloud formation.

RESULTS

Satellite observations

MSG-HRV data allows cloud cover patterns over Paris and London to be identified at high spatial and temporal resolution. Figure 1 (Supplementary Movie 1) is a MSG-HRV example for a typical cumulus (fair weather, low clouds) day in June 2010 over Paris. Initially, the day is clear with a northwesterly flow, cumulus clouds form during the morning and remain in the afternoon (Fig. 1b). In the evening more clouds remain over Paris than the surroundings (Fig. 1c) and stay active until after sunset above the city. This is a striking example of convective clouds lingering over Paris which occurs rather frequently.

To determine if this (Fig. 1) is an isolated case, multiple years (2009–2018) of MSG-HRV data are analysed during late-spring and summer (May, June, July, August). In the Paris region, the cloud fractions (Fig. 2a) are generally higher (mean of ~4.1% and a median of ~3.0% 14:00–17:00 UTC) over the urban surface when cumulus clouds are the dominant cloud class (>6 h per day, Methods section). In the morning the difference in cloud cover is small, but increases in the afternoon to a mean difference of 5.3% at 16:00 UTC. This analysis includes all pixels in the domain (Fig. 2c) with one land cover class (100%). Throughout the day, the cloud fractions are statistically significantly different (z-split,

¹Department of Meteorology, University of Reading, Reading, UK; ²Hydrology and Quantitative Water Management Group, Wageningen University & Research, Wageningen, the Netherlands and ³Institut Pierre Simon Laplace, Centre National de la Recherche Scientifique, Ecole Polytechnique, Palaiseau, France
Correspondence: Natalie E. Theeuwes (n.e.theeuwes@reading.ac.uk)

Received: 22 January 2019 Accepted: 1 May 2019

Published online: 24 May 2019

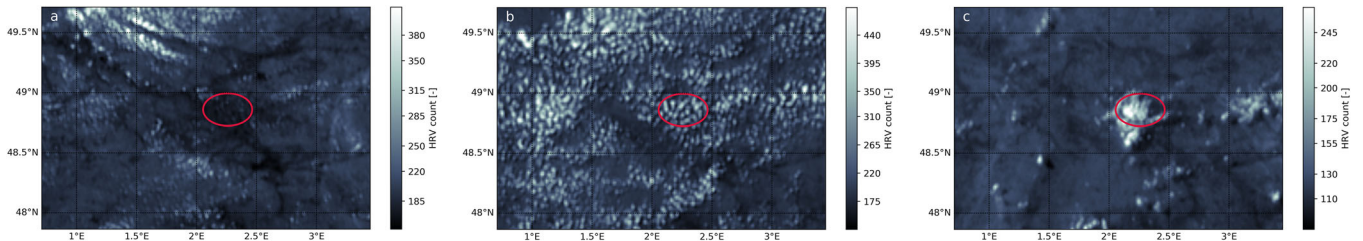


Fig. 1 High-resolution visible channel (HRV) images with clouds over Paris region. On 26 June 2010 at **a** 10:30 UTC **b** 14:00 UTC, **c** 17:30 UTC. The HRV count represents the reflected radiation within 0.4–1.1 μm waveband. The red oval has a 30 km long axis around the centre of Paris

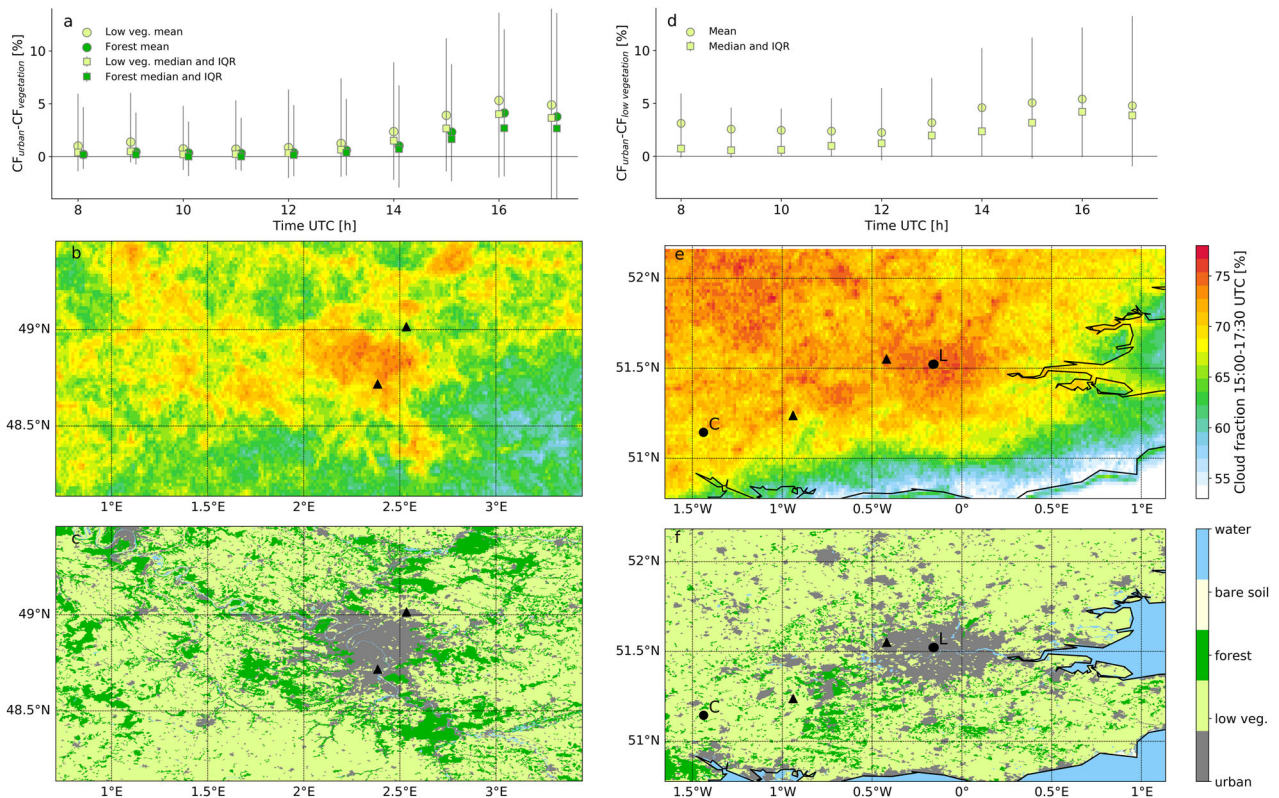


Fig. 2 Summer cloud cover over Paris and London regions. **a, d** The mean (circles) and median (squares) with the interquartile ranges (IQR, error bars) of the differences in cloud fraction between all urban pixels and all low-plant pixels (light green) and all forest pixels (dark green) for **a** Paris and **d** London. Only HRV pixels with 100% of one land cover type are analysed. **b, e** Afternoon (15:00–17:30 UTC) mean cloud fractions for **b** Paris and **e** London. **c, f** The CORINE land cover (250 m resolution)⁵³ for **c** Paris and **f** London. Data for days with a predominantly cumulus cloud class (see Methods) for 2009–2018 in May, June, July and August. (**e, f** dots) Locations of London and Chilbolton sites, (**b, c, e, f** triangles) airport sites used to select cumulus cases (Paris: $n_{\text{days}} = 563$, London: $n_{\text{days}} = 549$)

Wilcoxon sign-ranked test: $n_{\text{urban}} = n_{\text{low vegetation}} = 21,960$, $T = 90,529,747.5$ and $p = 0.000$ between urban and rural pixels. The interquartile ranges show the spread in the cloud fraction differences (Fig. 2a). Sometimes the differences are small, but an urban cloud fraction increment of 10–14% is frequent. Above Paris the mean cloud fraction is variable, 5–10% higher than over the surrounding areas, with a maximum over the northeast of the city (Fig. 2b). Other areas with enhanced cloud cover are large forest regions, which is in agreement with previous studies.²¹ Therefore, the magnitude of the difference (Fig. 2a) depends on which rural land cover type the urban fraction is compared to. The difference in cloud fraction (CF) relative to forests is smaller, as some enhancement of clouds is observed for both (median $CF_{\text{forest}} - CF_{\text{low vegetation}} = 0.7\%$). The orography in the area varies only slightly, with the largest elevation differences associated with the Seine river basin (~ 100 m, Supplementary Fig. 1). The smallest cloud fractions to the southeast of Paris coincide with a valley that might reduce convective activity.²²

To assess whether local mechanisms other than those associated with the city may cause the enhanced occurrence of clouds, the same analysis is performed for London (Fig. 2d–f). In London differences between urban and rural cloud fractions are slightly higher (mean of $\sim 5.0\%$ and a median of $\sim 3.4\%$ 14:00–17:00 UTC) and again significant (z-split, Wilcoxon sign-ranked test: $n_{\text{urban}} = n_{\text{low vegetation}} = 21,825$, $T = 72,600,869$ and $p = 0.000$). As for Paris, the urban enhancement of clouds peaks in the afternoon. Again the spread shows the likelihood of larger differences in the interquartile range. Surrounding London, there are insufficient forest pixels to compute cloud fraction differences. Compared to Paris, differences in cloud fractions are slightly positive in the morning for London. For London, it is more challenging to establish the rural background cloud conditions given the proximity of the coast and elevated terrain (Supplementary Fig. 1). The analysis (Fig. 2d) uses only those pixels in the domain (Fig. 2f) that are from a single (100%) land cover class and includes elevated pixels and those close to the coast. Near the

coast, the cloud fraction can be 10–15% lower than inland. This is attributed to the formation of an internal boundary layer as the surface transitions from sea to land. It takes about 10–20 km before the boundary layer reaches an equilibrium height.²³ Higher cloud fractions northwest of London are caused by orography (Supplementary Fig. 1).

Ground-based observations

As the MSG-HRV measurements require visible radiation, the cloud masks are unreliable during the evening transition. Hence, cloud occurrence (Fig. 3a) from ground-based ceilometer observations of cloud-base height (Fig. 3b) are analysed. The ceilometers are located in London and ~100 km to the south west (Chilbolton, Fig. 2f). The ceilometer data also show a higher frequency of clouds over London (Fig. 2a, d). During the afternoon (15:00–17:30) boundary-layer clouds are 7% more likely to occur over London than at Chilbolton. The enhanced London cloud frequency peaks at around 22:00 UTC, with cumulus clouds being 24% more common over the city than the rural site. This enhancement is found for all wind directions, but it is weaker when the wind is directly from the sea (Easterly to Northeasterly, Supplementary Fig. 2). A second peak in the cloud cover difference occurs around sunrise. However, this difference is not as apparent in the satellite data (Fig. 2d) and might be attributed to other mesoscale processes.

While there is enhanced occurrence of clouds over London in the afternoon and evening, the cloud-base height is higher during the day (Fig. 3b). The smallest differences in cloud-base height (London - Chilbolton) are observed at night when cloud-base

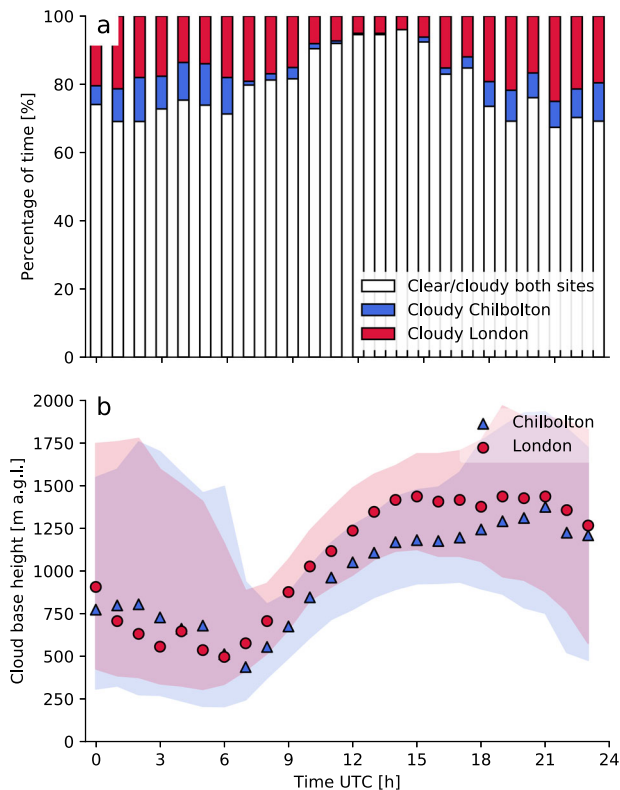


Fig. 3 Ceilometer-derived cloud occurrence and cloud base height (CBH). **a** Percentage of time with either clear or cloudy conditions at both sites (white), cloudy at Chilbolton and not over London (blue) and cloudy over London and not Chilbolton (red); **b** median CBH in m a.g.l. for cumulus days over London (red) and Chilbolton (blue) with interquartile ranges (shaded). Data for 2011–2015 and months May, June, July and August ($n_{\text{days}} = 268$)

height temporal variability is greatest. During the day variation in cloud-base height is smaller. Between the two sites the largest difference occurs 14:00–17:00 UTC, with a median difference of ~200 m. Higher cloud bases were observed in Nashville over the city in the afternoon¹⁰ and in California over more densely built urban surfaces for stratus clouds.²⁴ An elevated cloud base is associated with the presence of a drier sub-cloud layer causing the lifting condensation level (z_{LCL}) to be higher above the surface. The z_{LCL} is closely related to the dew-point depression at the surface (air minus dew point temperature, $T - T_d$).²⁵ A higher dew point depression indicates a drier sub-cloud layer and results in a greater cloud-base height. In May, June, July and August of 2011–2014 (all cumulus cases where the measurements of Chilbolton and London, overlap) the median afternoon (14:00–17:00) dew-point depression was 3.2 K higher in London (KCL) compared to Chilbolton. This is mostly driven by a much lower dew point temperature in the city (urban - rural $\Delta T_d = -2.5$ K and $\Delta T = 0.7$ K), demonstrating the reduced moisture in the city is largely responsible for the cloud-base height difference between London and Chilbolton.

Surface energy balance and boundary-layer turbulence

During spring and summer, the city has a drier atmosphere during the day than the surroundings.^{26–28} The decreased moisture over London can be attributed to the limited surface moisture available, causing latent heat fluxes to be about four times smaller than over the rural site during the day (Fig. 4).

Differences in turbulent sensible heat fluxes between the two sites are lowest in the morning, because in central London a larger proportion of the incoming energy is partitioned into the storage heat flux.¹⁴ After 11:00 UTC, the turbulent sensible heat flux at Chilbolton starts to decrease, becoming negative after 17:00 UTC. Whereas, in London, it starts to decrease 3 h later and usually stays around 50 W m^{-2} ,²⁹ providing persistent turbulent updrafts to transport the little available moisture upwards. These fluxes are

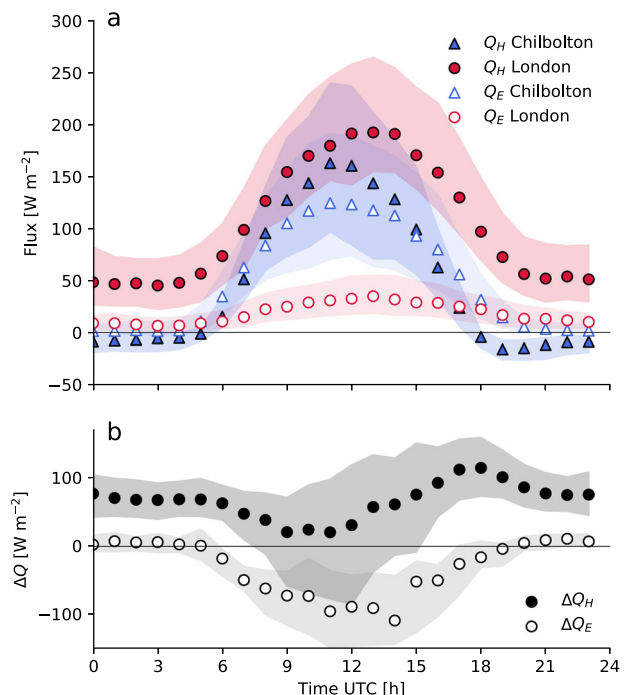


Fig. 4 Eddy covariance turbulent surface heat fluxes. **a** sensible (Q_H) and latent heat flux (Q_E) for London (KCL) and Chilbolton. **b** Median hourly differences in Q_H and Q_E medians and interquartile ranges (shading). For all cumulus days in May, June, July and August for years 2011–2014 ($n_{\text{days}} = 232$)

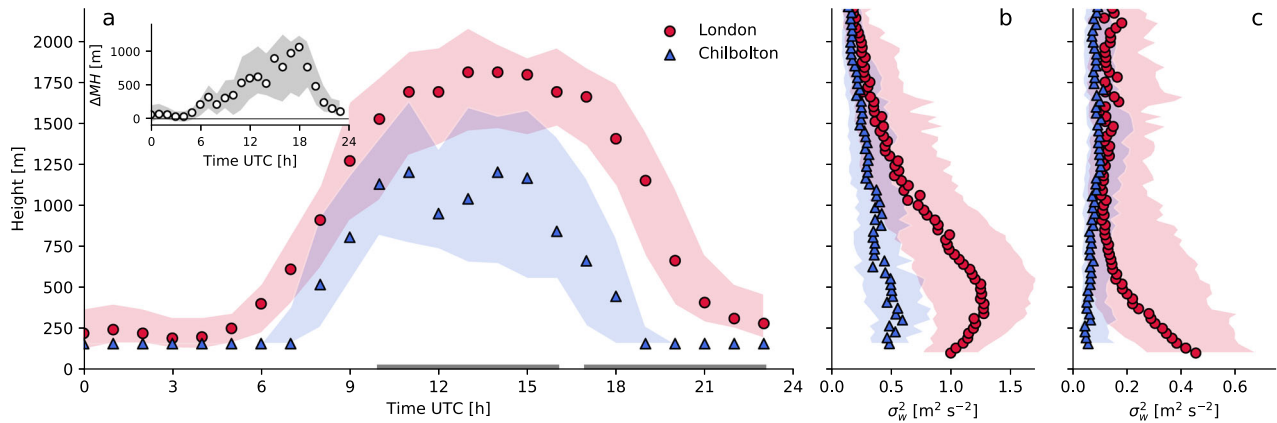


Fig. 5 Doppler lidar derived vertical velocity variance and mixing height. **a** Median mixing height (MH) and median hourly difference (ΔMH); (**b,c**) median vertical velocity variance between **b** 10:00 and 16:00 UTC and **c** 17:00 and 23:00 UTC for London at WCC (red) and Chilbolton (blue) with interquartile ranges (shaded). For available cumulus days between 1 May 2011 to 31 August 2011 ($n_{\text{days}} = 69$)

maintained by the release of storage heat flux from the built environment and hence continue to play a role even after sunset.

Longer-lasting surface-driven turbulence is confirmed by the vertical velocity variance derived from doppler lidar observations (Fig. 5c). During the day (10:00–16:00) the turbulence at both sites has a maximum above the ground, indicative of a convective boundary layer (driven by a positive Q_H). The velocity variance in the urban area is more than twice as strong as over the rural site (Fig. 5b). This results in a deeper day-time mixing height over London than over the rural site (Fig. 5a), as observed previously.^{10,30} The nocturnal higher sensible heat flux over London leads to increased vertical velocity variance (Fig. 5c). As a result, the sustained convection delays the decay of the mixing height (Fig. 5a) and sustains the clouds within the boundary layer. The clouds stay coupled to the surface moisture source longer and therefore persist into the night (Fig. 3a). Whereas, at the rural site the negative sensible heat flux results in the formation of a stable boundary layer, so that the convective clouds become decoupled from the surface and dissipate.

The source of the moisture that is transported upwards in the evening urban boundary layer is still unclear. In addition to moisture from the surface below (i.e., latent heat flux), surface heterogeneities in drag and energy balance partitioning could cause local circulations and horizontal convergence. This can transport moisture from other areas (e.g., parks).³¹ Zhu et al.⁸ found horizontal advection of rural moisture into the city depends on the soil moisture in the surroundings with clear effects on precipitation (and clouds) over the urban area.

The findings (Figs. 2–5) are robust, i.e., they do not depend on the case study periods selected. When all observations (ceilometer at Chilbolton and London, doppler lidar at Chilbolton and London, satellite images, and eddy covariance fluxes) overlap during the summer months of 2011 ($n_{\text{days}} = 69$), the same enhancement of clouds in the late afternoon and evening is observed in combination with a longer lasting positive sensible heat flux and greater mixing height over London compared to Chilbolton (Supplementary Fig. 3). This phenomenon is also illustrated in a case study (Supplementary Fig. 4).

DISCUSSION

The influence of the urban surface on cloud cover is similar to the enhancement seen over forests.^{21,32} This might seem counter-intuitive, but some of the near-surface processes in forests are similar to those in urban areas. Forests may be associated with higher sensible heat fluxes than from grasslands³³ depending on

the moisture availability at the sites. Additionally, forests can have enhanced surface drag and altered flow with potential influence on mesoscale circulations.³⁴

The extensive long-term data set in and around London allowed us to associate the persisting cloud cover to prolonged surface heating and convection over the city. Energy balance observations from many other cities have shown a longer lasting and mostly positive sensible heat flux during the evening and night time, including Basel, Switzerland,¹⁵ Marseille, France,³⁵ Helsinki, Finland,³⁶ Cairo, Egypt,³⁷ Łódź, Poland,³⁸ Montreal, Canada,³⁹ Mexico City, Mexico⁴⁰ and Sacramento, CA, USA.⁴¹ Hence, persistent convective clouds may occur over many large urban agglomerations.

Urban-precipitation interaction studies have also seen variations in precipitation patterns linked to surface heating,⁴² but hypothesise that not only the surface energy balance plays a role in altering convective precipitation over cities. The enhanced surface roughness/drag and additional aerosols acting as cloud condensation nuclei are also expected to influence convection, cloud formation and precipitation.^{16,43} There is still debate about the physical processes related to the influence of aerosols on cloud formation.⁴⁴ Aerosols are commonly suggested to enhance cloud lifetimes.⁴⁵ However, for low, non-precipitating clouds such as shallow cumulus the effect of enhanced aerosols on cloud lifetimes is observed to be very small or aerosols might even decrease their lifetime.^{46,47} The mechanisms responsible for linking urban surface fluxes to altered clouds and convection need to be confirmed using numerical simulations. Idealised simulations without synoptic forcing or aerosols have seen more persistent cloud cover over urban areas.⁸

For the boundary-layer clouds analysed here, the enhanced and longer lasting turbulent transport of moisture in the boundary layer driven by the extended sensible heat release over the city seems to cause clouds to be more persistent compared to rural settings. Therefore, urban areas are seen to directly affect weather phenomena besides temperature, impacting the city's inhabitants. Additionally, the difference in cloud cover is hypothesised to cause differences in the radiative forcing, especially during night time. A higher radiative forcing over the city could intensify the nocturnal urban heat island.

METHODS

A combination of observational tools are used in this study. The spatial variability in cloud cover is derived from satellite images. Cloud occurrence and cloud-base heights are derived from ceilometers.⁴⁸ Turbulence statistics and mixing heights are derived from a doppler lidar at a site in London and 100 km south west of London (Chilbolton 51°09'N, 01°26'W).

This study focuses on May, June, July and August, late spring and summer months.

Cumulus cases

The majority of the results are stratified to only include days with cumulus clouds present. Using SYNOP reports from two WMO stations in each city,⁴⁹ Orly (48.717°N; 2.384°E) and Charles de Gaulle (49.015°N; 2.534°E) for Paris and Northolt (51.549°N; -0.417°E) and Odiham (51.239°N; -0.9450°E) for London. All cloud types that occur for less than 6 h within a 24 h (0:00–0:00 UTC) period are excluded from the analysis. The day is classified by dominant cloud type. For the months May, June, July and August 2009–2018, there were days with cumulus present 44.8% in London and 45.2% of the time in Paris.

Satellite

Teuling et al.'s²¹ methodology is used to analyse MSG SEVIRI HRV broadband channel (0.4–1.1 μm) images to determine the presence of clouds at high resolution (~1 km). To reduce seasonal and diurnal variability effects from the surface albedo and solar zenith angle, while retaining sufficient data, cloud thresholds are calculated per pixel for hourly intervals using 10 days over the 10-year period (2009–2018). The 400 HRV counts per pixel (10 years \times 10 days \times 4 per hour) are sorted and the cumulative frequency distribution determined (example Supplementary Fig. 5). The spikes in the distribution are removed using a triangular moving average smoothing. The HRV count corresponding to the cloud threshold is taken as the next greater HRV count after the greatest difference of the consecutively ranked values in the cumulative distribution. Through this method the HRV counts that correspond to shadows are excluded. Using the cloud thresholds, cloud masks are created, where HRV-counts higher than the cloud threshold are classified as clouds and lower as clear. The cloud masks are used to determine the cloud fractions after which spatial (Fig. 2a, d) and temporal (Fig. 2b, e) statistics are calculated. Misclassified pixels due to underrepresentation of clear or cloudy HRV counts within an hour of a 10-day period might introduce errors into the statistics, but as these are individual pixels for a relatively small period of time and their effect is small relative to overall spatial results.

Ceilometer

Cloud occurrence probabilities and cloud-base height are determined from two Vaisala ceilometers (both operating at ~905 nm), a CL31 in London (MR, 51°31'21.1"N 0°09'16.5"W) and a CT75K at Chilbolton. The high-resolution data of the CL31 (15 s, 10 m) and CT25K (30 s, 30 m) are resampled to 15 min resolution according to Kotthaus and Grimmond.¹⁹ To focus on boundary-layer clouds, only cloud-base heights below 3 km are analysed. The five year (2011–2015) overlap between London and Chilbolton sites is analysed.

Fluxes

The turbulent sensible and latent heat fluxes are derived from eddy covariance measurements at Chilbolton and London (KCL 51°30'43.3"N 0°06'58.6"W). In Chilbolton the sonic anemometer (Metek USA-1) and open-path gas analyser (LICOR Li-7500) are mounted 5.3 m a.g.l. and sampled at 20 Hz.³⁰ In London, a CSAT3 (Campbell Scientific) sonic anemometer and a Li-7500A open path infrared gas analyser are mounted on a triangular tower, 48.9 m a.g.l. (until 2013) and 50.3 m a.g.l. (from 2013) (i.e., 2.2 times the mean building height), sampling at 10 Hz.²⁹ For both sites, 30-min fluxes are used for May, June, July and August 2011–2014.

Doppler lidar

A 1.5 μm HALO doppler lidar with 30 m vertical gates was located in London at Westminster City Council (WCC 51°31'16.31" N 0°09'38.33"W, 15 m a.g.l.) between 19 May 2011 and 11 January 2012. It was operated in vertical stare mode with a sampling frequency of 0.278 Hz. Data are available up to a height of 2415 m a.g.l.³⁰

A HALO doppler lidar with 36 m vertical gates was operated at Chilbolton at 1 m a.g.l. with a sampling frequency of 0.0256 Hz. Data are available to 9918 m a.g.l.⁵⁰

The first 3 gates are excluded for both lidars, and data with low signal to noise ratio is removed (SNR < -17 dB⁵¹). To correct for limited sampling frequency of the vertical velocity (w), a spectral correction is performed based on previous studies.^{30,50}

Using the corrected vertical velocity variance, the mixing height is determined assuming a threshold of $0.1 \text{ m}^2 \text{ s}^{-2}$. The sensitivity of this threshold is checked by perturbing the threshold by 30%^{20,30,52} within 21 bins. Finally, the median of the 21 values is chosen to be the mixing height. Mixing heights during periods (using the SYNOP reports) of rain are excluded from the analysis. This method of determining the mixing height is based on active turbulence in the boundary layer. A comparison to other, scalar-gradient methods of determining the mixed-layer height is discussed in Kotthaus et al.⁵²

DATA AVAILABILITY

Raw data for the Chilbolton site is available at <http://catalogue.ceda.ac.uk/>. MSG HRV channel data can be requested at <https://www.eumetsat.int/website/home/Data/ODegreeService/index.html>. The processed data and codes are available at <https://doi.org/10.5281/zenodo.2640662> by request.

ACKNOWLEDGEMENTS

This research was funded by an NWO Rubicon grant "Clouds above the city" (N.E.T.), EU H2020 URBANFLUXES (N.E.T., C.S.B.G) and Newton Fund/Met Office C5SP China (N. E.T., C.S.B.G, S.K.). Thanks to Christos Halios for sharing doppler lidar processing codes. Thanks to Rosy Wilson, Mike Stroud and John Lally for technical support during the ACTUAL project, to Steve Neville at Westminster City Council for permission to locate instrumentation at the WCC rooftop site. The ACTUAL Project was funded under Engineering and Physical Sciences Research Council Grant Number EP/G022938/1. LUMO has been funded by various NERC, EU7 and H2020 grants and supported by King's College London and University of Reading. For all field sites we thank the organizations that host the instruments and all the people that support the day-to-day operations.

AUTHOR CONTRIBUTIONS

N.E.T. designed research and carried out the data analysis; N.E.T., J.F.B., A.J.T. and C.S. B.G. analysed and interpreted the results; N.E.T. and S.K. processed the observations and all authors contributed to writing the paper.

ADDITIONAL INFORMATION

Supplementary information accompanies the paper on the *npj Climate and Atmospheric Science* website (<https://doi.org/10.1038/s41612-019-0072-x>).

Competing interests: The authors declare no competing interests.

Publisher's note: Springer Nature remains neutral with regard to jurisdictional claims in published maps and institutional affiliations.

REFERENCES

- United Nations. World urbanization prospects, the 2018 revision. *Tech. Rep.* <https://population.un.org/wup/> (2018).
- Oke, T. R. The energetic basis of the urban heat island. *Q. J. R. Meteorol. Soc.* **108**, 1–24 (1982).
- Arnfield, A. J. Two decades of urban climate research: a review of turbulence, exchanges of energy and water, and the urban heat island. *Int. J. Climatol.* **23**, 1–26 (2003).
- Theeuwes, N. E., Steeneveld, G.-J., Ronda, R. J. & Holtslag, A. A. A diagnostic equation for the daily maximum urban heat island effect for cities in north-western Europe. *Int. J. Climatol.* **37**, 443–454 (2017).
- Bornstein, R. & Lin, Q. Urban heat islands and summertime convective thunderstorms in Atlanta: three case studies. *Atmos. Environ.* **34**, 507–516 (2000).
- Zhong, S., Qian, Y., Zhao, C., Leung, R. & Yang, X.-Q. A case study of urbanization impact on summer precipitation in the Greater Beijing Metropolitan Area: Urban heat island versus aerosol effects. *J. Geophys. Res. Atmospheres* **120**, 10–903 (2015).
- Han, J.-Y. & Baik, J.-J. A theoretical and numerical study of urban heat island-induced circulation and convection. *J. Atmos. Sci.* **65**, 1859–1877 (2008).
- Zhu, X. et al. An idealized LES study of urban modification of moist convection. *Q. J. R. Meteorol. Soc.* **143**, 3228–3243 (2017).
- Romanov, P. Urban influence on cloud cover estimated from satellite data. *Atmos. Environ.* **33**, 4163–4172 (1999).
- Angevine, W. M. et al. Urban–rural contrasts in mixing height and cloudiness over Nashville in 1999. *J. Geophys. Res. Atmos.* **108** (2003).

11. Inoue, T. & Kimura, F. Urban effects on low-level clouds around the Tokyo metropolitan area on clear summer days. *Geophys. Res. Lett.* **31** (2004).
12. Betts, A. K., Ball, J. H., Beljaars, A., Miller, M. J. & Viterbo, P. A. The land surface-atmosphere interaction: A review based on observational and global modeling perspectives. *J. Geophys. Res. Atmos.* **101**, 7209–7225 (1996).
13. Ek, M. & Holtslag, A. Influence of soil moisture on boundary layer cloud development. *J. Hydrometeorol.* **5**, 86–99 (2004).
14. Grimmond, C., Cleugh, H. & Oke, T. An objective urban heat storage model and its comparison with other schemes. *Atmos. Environ. B. Urban Atmos.* **25**, 311–326 (1991).
15. Christen, A. & Vogt, R. Energy and radiation balance of a central European city. *Int. J. Climatol.* **24**, 1395–1421 (2004).
16. Shepherd, J. M. A review of current investigations of urban-induced rainfall and recommendations for the future. *Earth Interact.* **9**, 1–27 (2005).
17. Schmetz, J. et al. An introduction to Meteosat second generation (MSG). *Bull. Am. Meteorol. Soc.* **83**, 977–992 (2002).
18. Kotzeva, M. M. & Brandmüller, T. Urban Europe: statistics on cities, towns and suburbs. *Tech. Rep.* Publications office of the European Union (2016).
19. Kotthaus, S. & Grimmond, C. S. B. Atmospheric boundary-layer characteristics from ceilometer measurements. Part 1: A new method to track mixed layer height and classify clouds. *Q. J. R. Meteorol. Soc.* **144**, 1525–1538 (2018).
20. Halios, C. H. & Barlow, J. F. Observations of the morning development of the urban boundary layer over London, UK, taken during the ACTUAL project. *Bound.-Layer. Meteorol.* **166**, 395–422 (2018).
21. Teuling, A. J. et al. Observational evidence for cloud cover enhancement over western European forests. *Nat. Commun.* **8**, 14065 (2017).
22. Gibson, H. M. & Vonder Haar, T. H. Cloud and convection frequencies over the southeast United States as related to small-scale geographic features. *Mon. Weather Rev.* **118**, 2215–2227 (1990).
23. Angevine, W. Transitional, entraining, cloudy, and coastal boundary layers. *Acta Geophys.* **56**, 2–20 (2008).
24. Williams, A. P. et al. Urbanization causes increased cloud base height and decreased fog in coastal southern California. *Geophys. Res. Lett.* **42**, 1527–1536 (2015).
25. Lawrence, M. G. The relationship between relative humidity and the dewpoint temperature in moist air: a simple conversion and applications. *Bull. Am. Meteorol. Soc.* **86**, 225–234 (2005).
26. Hage, K. Urban-rural humidity differences. *J. Appl. Meteorol.* **14**, 1277–1283 (1975).
27. Ackerman, B. Climatology of Chicago area urban-rural differences in humidity. *J. Clim. Appl. Meteorol.* **26**, 427–430 (1987).
28. Ward, H. et al. Effects of urban density on carbon dioxide exchanges: Observations of dense urban, suburban and woodland areas of southern England. *Environ. Pollut.* **198**, 186–200 (2015).
29. Kotthaus, S. & Grimmond, C. S. B. Energy exchange in a dense urban environment—part I: Temporal variability of long-term observations in central London. *Urban Clim.* **10**, 261–280 (2014).
30. Barlow, J. F., Halios, C. H., Lane, S. & Wood, C. R. Observations of urban boundary layer structure during a strong urban heat island event. *Environ. Fluid Mech.* **15**, 373–398 (2015).
31. Kang, S.-L. & Bryan, G. H. A large-eddy simulation study of moist convection initiation over heterogeneous surface fluxes. *Mon. Weather Rev.* **139**, 2901–2917 (2011).
32. Wang, J. et al. Impact of deforestation in the Amazon basin on cloud climatology. *Proc. Natl Acad. Sci.* **106**, 3670–3674 (2009).
33. Teuling, A. J. et al. Contrasting response of European forest and grassland energy exchange to heatwaves. *Nat. Geosci.* **3**, 722–727 (2010).
34. Pielke, R. A. & Avissar, R. Influence of landscape structure on local and regional climate. *Landsc. Ecol.* **4**, 133–155 (1990).
35. Grimmond, C., Salmond, J., Oke, T. R., Offerle, B. & Lemonsu, A. Flux and turbulence measurements at a densely built-up site in Marseille: Heat, mass (water and carbon dioxide), and momentum. *J. Geophys. Res. Atmos.* **109**, (2004).
36. Nordbo, A., Järvi, L., Haapanala, S., Moilanen, J. & Vesala, T. Intra-city variation in urban morphology and turbulence structure in Helsinki, Finland. *Bound.-layer. Meteorol.* **146**, 469–496 (2013).
37. Frey, C. M., Parlow, E., Vogt, R., Harhash, M. & Wahab, M. M. A. Flux measurements in Cairo. Part 1: in situ measurements and their applicability for comparison with satellite data. *Int. J. Climatol.* **31**, 218–231 (2011).
38. Offerle, B., Grimmond, C. S. B., Fortuniak, K., Klysiak, K. & Oke, T. R. Temporal variations in heat fluxes over a central European city centre. *Theor. Appl. Climatol.* **84**, 103–115 (2006).
39. Bergeron, O. & Strachan, I. B. Wintertime radiation and energy budget along an urbanization gradient in Montreal, Canada. *Int. J. Climatol.* **32**, 137–152 (2012).
40. Oke, T. R., Spronken-Smith, R., Jáuregui, E. & Grimmond, C. S. The energy balance of central Mexico City during the dry season. *Atmos. Environ.* **33**, 3919–3930 (1999).
41. Cleugh, H. & Grimmond, C. Modelling regional scale surface energy exchanges and CBL growth in a heterogeneous, urban-rural landscape. *Bound.-Layer. Meteorol.* **98**, 1–31 (2001).
42. Dou, J., Wang, Y., Bornstein, R. & Miao, S. Observed spatial characteristics of Beijing urban climate impacts on summer thunderstorms. *J. Appl. Meteorol. Climatol.* **54**, 94–105 (2015).
43. Han, J.-Y., Baik, J.-J. & Lee, H. Urban impacts on precipitation. *Asia-Pac. J. Atmos. Sci.* **50**, 17–30 (2014).
44. Fan, J., Wang, Y., Rosenfeld, D. & Liu, X. Review of aerosol–cloud interactions: Mechanisms, significance, and challenges. *J. Atmos. Sci.* **73**, 4221–4252 (2016).
45. Charlson, R. J. et al. Climate forcing by anthropogenic aerosols. *Science* **255**, 423–430 (1992).
46. Jiang, H., Xue, H., Teller, A., Feingold, G. & Levin, Z. Aerosol effects on the lifetime of shallow cumulus. *Geophys. Res. Lett.* **33** (2006).
47. Small, J. D., Chuang, P. Y., Feingold, G. & Jiang, H. Can aerosol decrease cloud lifetime? *Geophys. Res. Lett.* **36**, L16806 (2009).
48. O'Connor, E. J., Illingworth, A. J. & Hogan, R. J. A technique for autocalibration of cloud lidar. *J. Atmos. Ocean. Technol.* **21**, 777–786 (2004).
49. WMO. Manual on codes. *WMO Publ. Tech. Rep.* **1** (1974).
50. Hogan, R. J., Grant, A. L., Illingworth, A. J., Pearson, G. N. & O'Connor, E. J. Vertical velocity variance and skewness in clear and cloud-topped boundary layers as revealed by doppler lidar. *Q. J. R. Meteorol. Soc.* **135**, 635–643 (2009).
51. Lane, S., Barlow, J. F. & Wood, C. R. An assessment of a three-beam Doppler lidar wind profiling method for use in urban areas. *J. Wind Eng. Ind. Aerodyn.* **119**, 53–59 (2013).
52. Kotthaus, S., Halios, C. H., Barlow, J. F. & Grimmond, C. Volume for pollution dispersion: London's atmospheric boundary layer during ClearFlo observed with two ground-based lidar types. *Atmos. Environ.* **190**, 401–414 (2018).
53. Bossard, M. et al. *Corine Land Cover Technical Guide: Addendum 2000*. Report No. 40/2000 (European Environment Agency, Denmark, 2000).



Open Access This article is licensed under a Creative Commons Attribution 4.0 International License, which permits use, sharing, adaptation, distribution and reproduction in any medium or format, as long as you give appropriate credit to the original author(s) and the source, provide a link to the Creative Commons license, and indicate if changes were made. The images or other third party material in this article are included in the article's Creative Commons license, unless indicated otherwise in a credit line to the material. If material is not included in the article's Creative Commons license and your intended use is not permitted by statutory regulation or exceeds the permitted use, you will need to obtain permission directly from the copyright holder. To view a copy of this license, visit <http://creativecommons.org/licenses/by/4.0/>.

© The Author(s) 2019